

Manuscript submission:

Title: Deactivation of Co-based Fischer-Tropsch catalyst by aerosol deposition of potassium salts

Short title: Deactivation of Co FTS catalyst by K

Authors:

Ljubiša Gavrilović, Norwegian University of Science and Technology, Department of Chemical Engineering, Sem Sælands vei 4, 7491 Trondheim, Norway

Jan Brandin, Linnæus University, Department of Built Environment and Energy Technology, 351 95 Växjö, Sweden

Anders Holmen, Norwegian University of Science and Technology, Department of Chemical Engineering, Sem Sælands vei 4, 7491 Trondheim, Norway

Hilde J. Venvik, Norwegian University of Science and Technology, Department of Chemical Engineering, Sem Sælands vei 4, 7491 Trondheim, Norway

R. Myrstad, SINTEF Materials and Chemistry, NO-7465 Trondheim, Norway

Edd A. Blekkan, Norwegian University of Science and Technology, Department of Chemical Engineering, Sem Sælands vei 4, 7491 Trondheim, Norway (corresponding author).

Corresponding author's e-mail address: edd.a.blekkan@ntnu.no

Keywords:

Fischer-Tropsch

Biomass

Cobalt catalyst

Deactivation

Potassium

Funding: The Research Council of Norway, contract no: 228741.

Abstract

A 20%Co/0.5%Re/ γ -Al₂O₃ Fischer-Tropsch catalyst was poisoned by four potassium salts (KNO₃, K₂SO₄, KCl, K₂CO₃) using the aerosol deposition technique, depositing up to 3500 ppm K as solid particles. Standard characterization techniques (H₂ Chemisorption, BET, TPR) showed no difference between treated samples and their unpoisoned counterpart. The Fischer-Tropsch activity was investigated at industrially relevant conditions (210 °C, H₂:CO = 2:1, 20 bar). The catalytic activity was significantly reduced for samples exposed to potassium, and the loss of activity was more severe with higher potassium loadings, regardless of the potassium salt used. A possible dual deactivation effect by potassium and the counter-ion (chloride, sulfate) is observed with the samples poisoned by KCl and K₂SO₄. The selectivity towards heavier hydrocarbons (C₅₊) was slightly increased with increasing potassium loading, while the CH₄ selectivity was reduced for all the treated samples. The results support the idea that potassium is mobile under FT conditions. The loss of activity was described by simple deactivation models which imply a strong non-selective poisoning by the potassium species.

1. Introduction

Fischer-Tropsch (FT) synthesis is an important technology for converting carbon-containing feedstocks (coal, natural gas, biomass) into liquid fuels and chemicals¹. Due to the chemistry of the Fischer-Tropsch synthesis and characteristics of the hydrocarbon products, the production of

diesel fuel and aviation fuel (jet fuel) is particularly attractive. FT diesel has better properties than the crude oil based fuels with respect to the cetane number and absence of aromatic and sulphur compounds². CTL (coal to liquid) and GTL (gas to liquid) are established industries, and there is a large and growing interest in developing BTL (biomass to liquid) processes³. Large scale BTL will probably utilize entrained flow gasification⁴, where the biomass is converted to syngas at temperatures above slagging (ash melting point), conditions where there is a significant vapour pressure of ash components. This necessitates gas cleaning and conditioning, process steps that add cost and reduce the thermal efficiency of the overall process. There is also a risk of errors in design or operation of the gas cleaning units, allowing the transport of inorganic impurities (e.g. Si, Ca, K, Na, S, Cl, Mg, Zn, Fe, Mn) to the downstream catalysts, e.g. the Co-based FTS catalyst in the synthesis part of the process⁵. Most of these elements are strong poisons for the Co based FT catalyst⁶. Several parameters influence the level of inorganic impurities, including the biomass feedstock (e.g. wood, straw), the gasifier technology (fluid bed, entrained flow), and the use of gasifier bed materials or additives (e.g. kaolin, dolomite, olivine) ⁷. The syngas cleaning can be done by conventional and hot gas cleaning⁸. Methods like cyclones, hot gas filters, granular beds are the main techniques involved in gas cleaning⁹. If a hot gas filter is implemented to remove the particulates, the impurity levels will also depend on the filtration conditions as well as temperature⁷. Alkali species can be present either in the gaseous form, condensed on the ash particles or as fine, submicrometer aerosol particles that might penetrate through the hot gas filter^{10,11}.

Potassium is usually the dominant alkali metal in biofuels, unlike in coal where sodium dominates¹². Pagels et al¹³ studied effluent gas composition emitted from biomass combustion

in small grate type boilers. Fine particles (around 100 nm) were produced with the elements K, S, and Cl, with the corresponding components being K_2SO_4 and KCl. Froment et al.¹⁴ performed thermodynamic equilibrium calculations during wood gasification and concluded that potassium will be semi-volatile in the form of hydroxide, carbonate and chloride. Which form potassium will take depends on the temperature inside the gasifier i.e. type of the gasifier and the melting temperature of the potassium salts. For the temperature of the autothermal Entrained Flow Reactor (EFR) (>1300°C) metallic K gaseous species appear in the 100 ppm vol. range.

Previous work in our group^{15, 16} has shown a strong negative effect of alkali and alkaline earth compounds on the catalyst activity of 20 wt% Co and 0.5 wt% Re on $\gamma-Al_2O_3$ catalysts during Fischer Tropsch synthesis. The compounds were introduced to the catalyst by incipient wetness impregnation of relevant, dissolved nitrates and subsequent calcination. A similar study was done by De la Osa et al.¹⁷, where a Co based FT catalyst was promoted with alkali and alkaline earth metals. The alkali was also introduced the by impregnation, however, onto the alumina support prior to the deposition of Co (20 wt%). The authors concluded that the potassium-promoted Co catalyst yielded lower CO conversion compared to the unpromoted one.

In order to better represent the actual gasification process, we have in this study adapted an aerosol deposition route to simulate gas-borne poisoning¹⁸. This route is essentially different from the hitherto applied impregnation routes¹⁵⁻¹⁷. Furthermore, taking into account the speciation of potassium based on the thermodynamic calculations mentioned above, four potassium salts (KNO_3 , K_2SO_4 , K_2CO_3 , and KCl) were chosen as representative poisons that can be found in biomass-based syngas.

The aerosol deposition technique has been used previously in similar work on a Ni catalyst in the SCR reaction¹⁹. Albertazzi et al.²⁰ also studied the impact of some of the contaminants from biomass gasification deposited on a homemade Pt-Rh/MgAl(O) reforming catalyst using the aerosol technique. The authors observed both a decreased total surface area and loss of metal dispersion and metallic surface area when the catalyst was exposed to aerosol particles of salts such as K₂SO₄ and ZnCl₂. The authors explained this behaviour as a simple geometrical blocking of the catalyst surface area by the above mentioned poisons.

Deactivating the Co catalysts by one potassium salt at a time helps in detailed understanding of the deactivation mechanisms for that salt, while in an actual BTL plant the catalyst will be exposed to the all emitted deactivation species at once²¹. The method used here, to poison the catalyst by aerosol deposition, will hopefully improve the understanding of how the alkali (potassium specifically) influences a Co-based F-T catalyst and provide a more realistic representation of the *in situ* poisoning. The knowledge obtained can be useful in designing future BTL plants, and the methodology can be expanded to represent more complex mixtures.

2. Experimental

2.1. Catalyst preparation

A standard 20%Co/0,5%Re/ γ alumina catalyst was used throughout these experiments. The metals were deposited on the support using a one-step incipient wetness impregnation of an aqueous

solution of $\text{Co}(\text{NO}_3)_2 \cdot 6\text{H}_2\text{O}$ and HReO_4 . The support was Puralox γ alumina from Sasol. After impregnation, the catalyst was dried in a stationary oven at 393K for 1h. To achieve homogeneity, the sample was stirred every 15 min. After drying, the catalyst was calcined in flowing air in a fixed bed quartz reactor at 573K for 16h (heating rate 2K/min). The final step was sieving the oxidized catalyst precursors to particles size 53-90 microns. The catalyst prepared like this is considered to be free from impurities, but the support did contain a minor amount of Na (26ppm)²².

2.2. Catalyst exposure by aerosol deposition of potassium salts

4 potassium salts (KNO_3 , K_2SO_4 , K_2CO_3 , and KCl) were deposited using the aerosol technology in the apparatus shown in Fig. 1²³. The salts were dissolved in deionized water inside the atomizer with the concentration of 0,025mol/dm³ of deionized water. The pneumatic atomizer produces aerosol particles from the solution. Nitrogen, used as a carrier gas, forces the generated aerosol particles towards the reactor. On the way to the reactor, the gas mixture containing the aerosol particles passes an impaction vessel, which separates and trap large particles. In this way a narrower particle size distribution is achieved.

The deposition experiments were performed at 300°C and 1bar. The tubular quartz reactor is placed inside the electrically heated oven with the catalyst bed is placed in the middle. The bottom of the catalyst bed is porous a glass frit, which allows the gas to pass through, while most of the aerosols remain on the catalyst. The gas flow was 4 l/min, and the catalyst bed was exposed to the aerosol-containing flow for three different times on stream, 15min, 60min and

300min. To achieve a very high K loading, one sample was prepared by using a stronger salt concentration (0.1mol/dm^3 of KNO_3 in deionized water) and the deposition time was increased to 7h. The drying time of the generated particles at these conditions is in the range of milliseconds, while the residence time of the gas in the oven is in the range of seconds²⁴. Considering melting points of the potassium salts and the experimental conditions used, the aerosol particles are completely dry and the salts are deposited in the form of solid particles on the catalyst.

The generated aerosol particles were physically characterized according to their electrical mobility using a scanning mobility particle sizer (SMPS) consisting of a differential mobility analyser (DMA, TSI Inc. Model 3081) and a condensation particle counter (CPC) (TSI Inc. Model 3010)^{23,24}. The SMPS system was used to measure the particle size in the range from ~20 to 700 nm. A software package with an inversion algorithm converts the penetration characteristics (aerosol flow of around 0,3l/min) to the particle size distribution. Before entering to the SMPS system, the flow has been dried by a Nafion dryer (Perma Pure Inc., US). To prevent the entrance of larger particles into the system, an impactor device with a cut off size of 805nm was placed right before the SMPS system. Further treatment was done *in situ*.

Figure 1. *Experimental setup for catalyst exposure to the aerosol particles at 300°C*

2.3. Catalyst characterization

2.3.1. Nitrogen adsorption/desorption

Volumetric adsorption of N₂ was performed on a Tristar II 3020 to determine surface area, pore volume and average pore diameter of the support materials and prepared catalysts. Before the measurement at liquid nitrogen temperature, the samples (~70mg, particle size 53-90µm) were outgassed in vacuum, first at ambient temperature for 1h and then at 473K overnight. The Brunauer-Emmet-Teller (BET)²⁵ isotherm was used for calculation of the surface area and the Barret-Joyner-Halenda (BJH)²⁶ method was applied to determine pore volumes and average pore diameters of the samples. For the pore size analysis the nitrogen desorption branch was chosen²⁷.

2.3.2. H₂-chemisorption

H₂-chemisorption was performed using a Micromeritics ASAP2010 unit. The catalyst sample (0.2 g) was loaded in the chemisorption reactor, placed between two wads of quartz wool. Prior to chemisorption, the sample was heated (ramping rate of 60 K/h) from ambient temperature to 623 K and treated with flowing hydrogen at this temperature for 16 h. The sample was then cooled to 313 K under vacuum. Chemisorption data were collected at 313 K between 0.020 and 0.667 bar H₂ pressure. It was assumed that each surface cobalt atom was one H chemisorption site and that neither Re, K impurities or the support contributed to the chemisorption.

2.3.3. Temperature programme reduction

Temperature programme reduction (TPR) experiments were performed in an Altamira AMI-300RHP. The catalyst sample (150 mg) was loaded in a quartz u-tube reactor between wads of quartz wool. The catalyst was first treated in inert gas at 200°C and then reduced in hydrogen

flow (7% H₂/Ar, 50ml/min) to a temperature of 900°C with a ramp rate of 10°C/min. After reaching the final temperature, samples were cooled down to room temperature.

2.4. Fischer–Tropsch synthesis

Fischer–Tropsch synthesis was carried out in four parallel 10 mm ID steel tube fixed bed reactors at 483 K, 20 bar pressure with a H₂/CO ratio of 2.1. The samples (1 g) were diluted with inert SiC (20 g, particle size 53-90µm) to improve heat distribution and loaded between quartz wool wads to keep the catalyst in place. To further improve heat distribution, aluminium blocks were fixed around the reactors and the reactors were placed in four separate electrical furnaces. After leak tests with He the pressure was kept at 1.5 bar and flowing H₂ was introduced. To reach the reduction temperature of 623K, the samples were heated with a ramping rate of 1 K/min, and kept at 623 K for 16 h. After reduction, the samples were cooled to 443 K. Before introduction of syngas, the reactors were pressurized with He to the operating pressure of 20 bar. Following the introduction of the syngas (250 Nml/min), the temperature was increased to 463 K with a ramping rate of 20 K/min and then to the desired reaction temperature of 483 K with a ramping rate of 5 K/min. The condensable Fischer-Tropsch products, wax, lighter hydrocarbons and the water phase were collected in a hot trap at ~360 K and a cold trap at ambient temperature, respectively. Gas phase products were analyzed using an on-line HP 6890 gas chromatograph with a GS-Alumina PLOT column, TCD and a flame ionization detector (FID). The synthesis gas contained 3% N₂ which served as an internal standard for quantification of the products to create a mass balance. After ~24 h time-on-stream (TOS), activity data is reported based on measurements at a constant feed rate (250 Nml/min). Thereafter, the feed rate of synthesis gas

was adjusted to obtain ~50% CO conversion. Selectivity data are reported after ~48 h TOS at 50 ± 5% CO conversion based on the analysis of C₁–C₄ hydrocarbons in the gas phase from. Since the focus is on the amount of higher hydrocarbons, the selectivity is reported in the usual way as C₅+ and CH₄ selectivity.

Results and discussion

3.1 Physical characterization of aerosol particles

The generated aerosol particles from potassium salts have been characterized by SMPS (in the range ~20– 700 nm). Figure 2. shows the mass size distribution ($\mu\text{g}/\text{m}^3$) of generated aerosol particles plotted against the mean value of the mass diameter (nm). The obtained average value of particle mass diameters is around 210nm, 228nm, 228nm and 206nm for KCl, K₂CO₃, K₂SO₄ and KNO₃ respectively. The mass concentrations of 12.1 mg/Nm³, 8.7 mg/Nm³, 10.0 mg/Nm³, 12.7 mg/Nm³ are calculated based on the bulk density of 2 g/cm³, 2.43 g/cm³, 2.66 g/cm³, 2.1 g/cm³ for KCl, K₂CO₃, K₂SO₄ and KNO₃, respectively. All obtained results are presented at standard conditions: 0 °C and 1.01 × 10⁵ Pa, taking into account the dilution factor and assuming spherical particles.

Figure 2. *Mass size distribution of aerosol particles of potassium salts*

3.2. Characterization results

Key characterization results are shown in Table 1. Inductively coupled plasma (ICP-MS) was used to determine the ppm levels of potassium. The reference sample did not show potassium. All the treated samples showed increasing potassium content with increasing deposition time. The

sample which was prepared differently yielded a potassium concentration of 3530ppm. Catalyst morphological characteristics showed no significant difference—all the treated samples have about the same surface area (127-136m²/g), pore volume (0,45-0,47cm³/g) and pore size (13,1-13,6nm). Although there are minor differences between the samples, these variations are within experimental error. Temperature programmed reduction profiles of the reference Co-based catalyst and the catalysts poisoned with KCl are shown in Fig 3. The TPR profiles for the other potassium salts are similar and thus not presented here. All the poisoned samples show a reduction profile typical for alumina supported Co catalysts²⁸. The two main peaks at ~303°C and ~403°C are referred to the transition from Co₃O₄ to CoO and CoO to metallic Co, respectively^{18,28}. The initial shoulder on the first peak, appearing at approximately 200 °C represents the reduction of residual cobalt nitrate²⁹, which is left from catalyst preparation. To conclude, the samples containing potassium display similar reduction behaviour as the reference (potassium free) sample, with the same major peaks for the two reduction steps.

There is also no significant change in the chemisorption results, regardless of potassium level or potassium salt. All the poisoned samples show the same dispersion as the reference catalyst (7,6%). It was previously reported that addition of small amount of alkali elements dramatically reduced catalyst activity while the dispersion remain the same¹⁶. This work provides a similar result, since in the wide range of potassium loadings and using different potassium salts, the dispersion remains unchanged. The influence of K on cobalt surfaces has been investigated previously, e.g. was a monolayer of K on Co(0001) found to influence the adsorption of acetylene through a new adsorption state and also lead to a change in the formation of coke, especially graphitic carbon³⁰. Recent DFT work in our group indicated K atoms to be mobile on the most

relevant Co facets but not across steps and edges, thereby likely deactivating sites central to the activity of the Co particles under reaction conditions³¹. Furthermore, investigating Co(11-20) as an experimental model system we found that small amounts of metallic K deposited by evaporation is mobile at ambient temperature and prefers step edge locations on the surface³². The amount of adsorbed CO was reduced due to K, and this was associated with the CO-induced restructuring proceeding on this surface being obstructed by the K. Brown et al.³³ observed lower rate of D₂ dissociation when Pt (111) is promoted with K, explaining this as a long range electronic effect. Bonzel et al.³⁴ explained decrease in CO hydrogenation due to the electronic effect by K. In contrast, we see no effect on the hydrogen chemisorption following the aerosol deposition of K, similar to the results reported previously following incipient wetness impregnation of K^{16,35}. Thus, our results must be interpreted to indicate that following deposition, the K salts are not located on the cobalt particles, but probably as separate particles on the external surface of the catalyst.

Table 1. Catalysts prepared with the indicated potassium salt impurities and loadings

Figure 3. *TPR profiles of temperature vs hydrogen consumption of standard catalyst and catalysts with different potassium loadings*

3.3. Fischer-Tropsch Synthesis

Fischer-Tropsch activity results, presented as STY (site time yield) against potassium impurity loading, are plotted in Figure 4. The results are reported after 24h time on stream (TOS) with a constant feed-rate of 250 ml/min. A decreasing trend in catalyst activity with increasing potassium concentration is observed for all the samples, regardless of potassium precursors. The

samples treated with K_2SO_4 and KCl showed a steeper decline in catalyst activity with the K concentration when compared with K_2CO_3 and KNO_3 , indicating that the counter-ion also can play a role in the catalyst deactivation. From previous work it is known that S is a strong poison for cobalt based FT catalyst³⁶. Borg et al.³⁷ investigated the influence of chlorine on Co FT catalyst, and found no significant influence on activity or selectivity with chlorine loadings up to 800 ppm. In the present work KCl and K_2SO_4 appear to have a stronger effect than KNO_3 , indicating that the anion part of the salt also contributes to the decrease in activity. The deactivation effect decreases in the following order: $K_2SO_4 > KCl > K_2CO_3 > KNO_3$. The melting point of the potassium salts are K_2SO_4 (1069°C) > K_2CO_3 (890°C) > KCl (770°C) > KNO_3 (334°C). If the transport of the salt to the cobalt surface is an important factor, and the melting point is a measure of the mobility of the salt, the salt with the lowest (physical) mobility has the strongest negative effect on the catalyst. This could indicate not only that the strong deactivation behaviour by K_2SO_4 is an effect of K and the sulphate, but also that the transport of K is not related to melting the salt and liquid transport into the pore system. This is in agreement with the effect observed by Moradi et al.¹⁰ where a Pt catalyst was investigated in the Selective Catalytic Reduction (SCR) reaction.

Fischer-Tropsch selectivity measurements are reported at 50% conversion after ~48h time on stream, and the results are shown in Figures 5-9. All the treated samples show moderate increases in selectivities towards C_{5+} , CO_2 , and also in the C_3 olefin/paraffin ratio (O/P) and the C_4 O/P ratio. There was also a slight decrease in the selectivity to CH_4 with increasing potassium loading. The sample with the highest amount of potassium loading confirms these trends. This is

in agreement with the previous work where Co catalyst was poisoned with the series of alkali metals using incipient wetness impregnation¹⁶.

Potassium location plays an important role in explaining catalyst deactivation by alkali. The generated aerosol particles (Fig. 2) have dimensions much larger than the average pore size of the catalyst (Table 1), so they will be deposited on the external surface of the support. The deposition does not lead to measurable changes in the physical or chemical characteristics of the samples, indicating that the aerosol particles are neither blocking pores nor extensively covering cobalt sites. The effect on the catalytic activity is, however, profound. This would indicate that the potassium species are mobile under reaction conditions, and the significant partial pressure of water could play a role in the transport mechanism, similar to the effect observed following impregnation of potassium on the catalyst^{15,16,35}. This could, however, be interpreted to mean that the impregnated potassium species is not in close contact with the cobalt, but rather on the support, e.g. on acid sites. This possible transport of potassium and change in the catalytic activity must happen quite fast, during the initial stage of FT reaction where we do not monitor in the present set up changes in the activity (see Fig. S1). The presence of water, an important FT reaction product, could be a facilitator for this process. Recent DFT-calculations indicate that once potassium reaches the cobalt surface it is very mobile, and will probably migrate to occupy the most favourable sites which are on stepped facets³¹. Recent STM and DFT results show a similar picture, and STM demonstrates that the adsorbed K inhibits the adsorption-induced restructuring of the cobalt surface believed to be important for the catalytic activity³².

Figure 4. *Site time yield (STY) after 24h time on stream (TOS) with different potassium salts and loadings*

Figure 5. C_{5+} selectivity at 50% of conversion with different potassium salts and loadings

Figure 6. CH_4 selectivity at 50% of conversion with different potassium salts and loadings

Figure 7. CO_2 selectivity at 50% of CO conversion with different potassium salts and loadings

Figure 8. C_3 O/P selectivity at 50% of CO conversion with different potassium salts and loadings

Figure 9. C_4 O/P selectivity at 50% of CO conversion with different potassium salts and loadings

3.4. Kinetic modeling of deactivation data

In order to be able to predict the catalyst deactivation with potassium, the activity data previously presented were kinetically analyzed. The proposed simple (power rate law) kinetic model by Zennaro et al.³⁸ developed for a supported cobalt catalyst is given in (1) :

$$r_{CO} = k^o p_{H_2}^{0.74} p_{CO}^{-0.24} \quad (1)$$

In expression (1), r_{CO} (ml/h/gcat) is the rate of CO consumption; p_{H_2} , p_{CO} (Pa) are the partial pressures of reactants and k^o (ml/h/Pa^{0.5}/gcat) is the kinetic constant. To be able to predict the catalyst deactivation with potassium, the expression (1) was modified with a term in the expression of the kinetic constant depending on the K loading:

$$k = k^o f(K)$$

where K is the potassium concentration on the catalyst. Three simple empirical equations were selected from the work by Visconti et al.³⁹ to determine the effect of potassium on the catalyst activity (Table 2). In this table K is the potassium impurity loading expressed in mg_K/kg_{cat}, and k^o is the kinetic constant of the reference sample. The estimated value of k^o was the same for all

the expressions and it was set at the value obtained for the unpoisoned catalyst (0,775 ml/h/Pa^{0.5}/g_{cat}). The value of the parameters m was estimated by means of a linear regression of CO conversion data (see Fig. 4). In Table 2 we report the estimates of the adaptive parameters for the adopted deactivation kinetics together with the corresponding obtained relative error (RE) and the determination coefficient (R^2). Fig. 10 indicates that all the models fit the experimental results relatively well, however the best fit was found for model (3). However, the number of data-points is low, so the apparent agreement does not constitute evidence of a mechanism, but rather the result can be used as a tool to predict the effect of potassium on the surface.

Figure 10. Plots for the deactivation rate equations (1) (2) and (3). The straight lines represent linear regression to fit the results to the equation.

Conclusion

The current study presents findings from experimental work investigating the interaction between alkali salts in the form of aerosol particles and a Co-based FT catalyst investigated under industrially relevant conditions. Four potassium salts (KNO_3 , KCl , K_2CO_3 , K_2SO_4) were selected based on reported thermodynamic calculations of the effluent gas composition after biomass gasification. The activity measurements showed a severe drop in activity for all samples which were treated with potassium salts, regardless which potassium salt was used. The sample with

the highest amount of potassium showed a loss of 30% compared to the unpoisoned sample. Selectivity data were only slightly affected with an observed tendency in increasing S_{C_5+} , S_{CO_2} and decreasing S_{CH_4} with increasing potassium loading. A key finding is that none of the characterization techniques employed showed any differences between poisoned and unpoisoned sample, regardless of potassium salt. The results indicate that potassium mobility plays an important role in catalyst deactivation, where potassium after deposition does not influence the cobalt properties as observed during characterization, but still has a profound effect on the catalytic activity. This indicates that K is mobile, and is able to reach and influence specific sites for the FT reaction. Finally, three different deactivation models were described regarding the experimental data of CO conversion decay with K-loading. It can be concluded that the experimental results could be adequately described by a simple kinetic deactivation model which indicates a strong negative effect of K on the reaction rate.

Acknowledgements

We thank The Research Council of Norway for funding under the ENERGIX programme (contract no: 228741).

Supporting information

Plot showing time-dependent activity for the reference and following aerosol deposition of 3500 ppm K as KNO_3 .

References

- (1) Tijmensen, M. J. A.; Faaij, A. P. C.; Hamelinck, C. N.; Van Hardeveld, M. R. M. Exploration of the possibilities for production of Fischer Tropsch liquids and power via biomass gasification. *Biomass and Bioenergy* **2002**, *23*, 129–152.
- (2) Boerrigter, H.; Calis, H. P. Green Diesel from Biomass via Fischer-Tropsch synthesis: New Insights in Gas Cleaning and Process Design. *Pyrolysis and Gasification of Biomass and Waste*; **2002**.
- (3) Rauch, R.; Kiennemann, A.; Sauciuc, A. Fischer-Tropsch Synthesis to Biofuels (BtL Process). In *The Role of Catalysis for the Sustainable Production of Bio-Fuels and Bio-Chemicals*; K. Triantafyllidis, A. Lappas, M. Stöcker, Eds., Elsevier, **2013**, pp. 397–443.
- (4) Ail, S. S.; Dasappa, S. Biomass to liquid transportation fuel via Fischer Tropsch synthesis - Technology review and current scenario. *Renew. Sustain. Energy Rev.* **2016**, *58*, 267–286.
- (5) Li, Y. P.; Wang, T. J.; Wu, C. Z.; Gao, Y.; Zhang, X. H.; Wang, C. G.; Ding, M. Y.; Ma, L. L. Effect of Alkali Vapor Exposure on Ni-MgO/ γ -Al₂O₃/Cordierite Monolithic Catalyst for Biomass Fuel Gas Reforming. *Ind. Eng. Chem. Res.* **2010**, *49*, 3176–3183.
- (6) Tsakoumis, N. E.; Rønning, M.; Borg, Ø.; Rytter, E.; Holmen, A. Deactivation of cobalt based Fischer–Tropsch catalysts: A review. *Catalysis Today* **2010**, *154*, 162–182.
- (7) Moud, P. H.; Andersson, K. J.; Lanza, R.; Pettersson, J. B. C.; Engvall, K. Effect of gas phase alkali species on tar reforming catalyst performance: Initial characterization and method development. *Fuel* **2015**, *154*, 95–106.
- (8) Boerrigter, H.; Calis, H. P.; Slor, D. J.; Bodenstaff, H. Gas Cleaning for Integrated Biomass Gasification (BG) and Fischer-Tropsch (FT) Systems. *2nd World Conf. Technol. Exhib. Biomass*

Energy, Ind. Clim. Prot. **2004**, 10–14.

- (9) Simeone, E.; Siedlecki, M.; Nacken, M.; Heidenreich, S.; De Jong, W. High temperature gas filtration with ceramic candles and ashes characterisation during steam–oxygen blown gasification of biomass. *Fuel* **2013**; 108, 99–111.
- (10) Moradi, F.; Brandin, J.; Sohrabi, M.; Faghihi, M.; Sanati, M. Deactivation of oxidation and SCR catalysts used in flue gas cleaning by exposure to aerosols of high- and low melting point salts, potassium salts and zinc chloride. *Appl. Catal. B Environ.* **2003**, 46, 65–76.
- (11) Christensen, K. A.; Stenholm, M.; Livbjerg, H. The formation of submicron aerosol particles, HCl and SO₂ in straw-fired boilers. *Journal of aerosol science.* **1998**, 29,421-444
- (12) Kling, Å.; Andersson, C.; Myringer, Å.; Eskilsson, D.; Järås, S. G. Alkali deactivation of high-dust SCR catalysts used for NO_x reduction exposed to flue gas from 100MW-scale biofuel and peat fired boilers: Influence of flue gas composition. *Appl. Catal. B Environ.* **2007**, 69, 240–251.
- (13) Pagels, J.; Strand, M.; Rissler, J.; Szpila, A.; Gudmundsson, A.; Bohgard, M.; Lillieblad, L.; Sanati, M.; Swietlicki, E. Characteristics of aerosol particles formed during grate combustion of moist forest residue. *J. Aerosol Sci.* **2003**, 34, 1043–1059.
- (14) Froment, K.; Defoort, F.; Bertrand, C.; Seiler, J. M.; Berjonneau, J.; Poirier, J. Thermodynamic equilibrium calculations of the volatilization and condensation of inorganics during wood gasificatio. *Fuel* **2013**, 107, 269–281.
- (15) Balonek, C. M.; Lillebø, A. H.; Rane, S.; Rytter, E.; Schmidt, L. D.; Holmen, A. Effect of Alkali Metal Impurities on Co–Re Catalysts for Fischer–Tropsch Synthesis from Biomass-Derived Syngas. *Catal. Letters* **2010**, 138, 8–13.

- (16) Lillebø, A. H.; Patanou, E.; Yang, J.; Blekkan, E. A.; Holmen, A. The effect of alkali and alkaline earth elements on cobalt based Fischer–Tropsch catalysts. *Catalysis Today* **2013**, 215, 60–66.
- (17) De La Osa, A. R.; De Lucas, A.; Valverde, J. L.; Romero, A.; Monteagudo, I.; Coca, P.; Sánchez, P. Influence of alkali promoters on synthetic diesel production over Co catalyst. *Catalysis Today* **2011**, 167, 96–106.
- (18) Gavrilovic, L.; Brandin, J.; Holmen, A.; Venvik, H. J.; Myrstad, R.; Blekkan E. A. Fischer-Tropsch Synthesis – investigation of the deactivation of a Co catalyst by exposure to aerosol particles of potassium salt submitted to *Appl. Catal. B Environ.* **2017**
- (19) Albertazzi, S.; Basile, F.; Brandin, J.; Einvall, J.; Fornasari, G.; Hulteberg, C.; Sanati, M.; Trifirò, F.; Vaccari, A. Effect of fly ash and H₂S on a Ni-based catalyst for the upgrading of a biomass-generated gas. *Biomass and Bioenergy* **2008**, 32, 345–353.
- (20) Albertazzi, S.; Basile, F.; Brandin, J.; Einvall, J.; Fornasari, G.; Hulteberg, C.; Sanati, M.; Trifirò, F.; Vaccari, A. Pt-Rh/MgAl(O) Catalyst for the Upgrading of Biomass-Generated Synthesis Gases. *Energy and Fuels* **2009**, 23, 573–579.
- (21) Larsson, A.-C.; Einvall, J.; Sanati, M. Deactivation of SCR Catalysts by Exposure to Aerosol Particles of Potassium and Zinc Salts. *Aerosol Science and Technology*, 2007, 41, 369–379.
- (22) Borg, Øyvind; Eri, S.; Blekkan, E. A.; Storsæter, S.; Wigum, H.; Rytter, E.; Holmen, A. Fischer–Tropsch synthesis over γ -alumina-supported cobalt catalysts: Effect of support variables. *J. Catal.* **2007**, 248, 89–100.
- (23) Einvall, J.; Albertazzi, S.; Hulteberg, C.; Malik, A.; Basile, F.; Larsson, A. C.; Brandin, J.; Sanati, M. Investigation of Reforming Catalyst Deactivation by Exposure to Fly Ash from Biomass Gasification in Laboratory Scale. *Energy and Fuels* **2007**, 21, 2481–2488.

- (24) Hinds, W. C. *Aerosol technology: properties, behavior, and measurement of airborne particles*; John Wiley & Sons, **1999**.
- (25) Brunauer, S.; Emmett, P. H.; Teller, E. Adsorption of Gases in Multimolecular Layers. *J. Am. Chem. Soc.* **1938**, *60*, 309–319.
- (26) Barrett, E. P.; Joyner, L. G.; Halenda, P. P. The Determination of Pore Volume and Area Distributions in Porous Substances. I. Computations from Nitrogen Isotherms. *J. Am. Chem. Soc.* **1951**, *73*, 373–380.
- (27) Lowell, S.; Shields, J. E.; Thomas, M. A.; Thommes, M. Characterization of Porous Solids and Powders: Surface Area, Pore Size and Density; Particle Technology Series; *Springer Netherlands: Dordrecht*, **2004**; Vol. 16.
- (28) Rønning, M.; Tsakoumis, N. E.; Voronov, A.; Johnsen, R. E.; Norby, P.; Van Beek, W.; Borg, Ø.; Rytter, E.; Holmen, Combined XRD and XANES studies of a Re-promoted Co/g-Al₂O₃ catalyst at Fischer–Tropsch synthesis conditions. *A. Catal. Today* **2010**, *155*, 289–295.
- (29) Bao, A.; Li, J.; Zhang, Y. Effect of barium on reducibility and activity for cobalt-based Fischer–Tropsch synthesis catalysts. *J. Nat. Gas Chem.* **2010**, *19*, 622–627.
- (30) Vaari, J.; Lahtinen, J.; Hautajarvi, P. The adsorption and decomposition of acetylene on clean and K-covered Co(0001). *Catal. Lett.* **1997**, *44*, 43–49.
- (31) Chen, Q.; Svenum, I.; Qi, Y.; Gavrilovic, L.; Chen, D.; Holmen, A.; Blekkan, E. A.; Rytter, E.; Graham, U. M.; Thomas, G. A.; Davis, B. H. Potassium adsorption behavior on hcp cobalt as model systems for the Fischer–Tropsch synthesis: a density functional theory study. *Phys. Chem. Chem. Phys.* **2017**, *92*, 17–24.

- (32) Strømsheim, M. D.; Svenum, I. H.; Farstad, M. H.; Li, Z.; Gavrilovic, L.; Guo, X.; Lervold, S.; Borg, A.; Venvik, H. J. Effects of K adsorption on the CO-induced restructuring of Co(11-20). *Catal. Today* **2018**, *299*, 37-46.
- (33) Brown, J. K.; Luntz, A. C.; Schultz, P.A. Long-range poisoning of D₂ dissociative chemisorption on Pt(111) by coadsorbed K. *J. Chem. Phys.* **1991**, *95*, 3767-3774.
- (34) Bonzel, H. P.; Brodén, G.; Krebs, H. J. X-ray photoemission spectroscopy of potassium promoted Fe and Pt surfaces after H₂ reduction and CO/H₂ reaction. *Appl. Surf. Sci.* **1983**, *16*, 373-394.
- (35) Patanou, E.; Lillebø, A. H.; Yang, J.; Chen, D.; Holmen, A.; Blekkan, E. A. Microcalorimetric Studies on Co-Re/γ-Al₂O₃ Catalysts with Na Impurities for Fischer-Tropsch Synthesis. *Ind. Eng. Chem. Res.* **2014**, *53*, 1787-1793.
- (36) Barrientos, J.; Montes, V.; Boutonnet, M.; Järås, S. Further insights into the effect of sulfur on the activity and selectivity of cobalt-based Fischer-Tropsch catalysts. *Catal. Today* **2016**, *275*, 119-126.
- (37) Borg, Ø.; Hammer, N.; Enger, B. C.; Myrstad, R.; Lindvg, O. A.; Eri, S.; Skagseth, T. H.; Rytter, E. Effect of biomass-derived synthesis gas impurity elements on cobalt Fischer-Tropsch catalyst performance including in situ sulphur and nitrogen addition. *J. Catal.* **2011**, *279*, 163-173.
- (38) Zennaro, R.; Tagliabue, M.; Bartholomew, C. H. Kinetics of Fischer-Tropsch synthesis on titania-supported cobalt. *Catal. Today* **2000**, *58*, 309-319.
- (39) Visconti, C. G.; Lietti, L.; Forzatti, P.; Zennaro, R. Fischer-Tropsch synthesis on sulphur poisoned Co/Al₂O₃ catalyst. *Appl. Catal. A Gen.* **2007**, *330*, 49-56.

Table 1. Catalysts prepared with salt impurities and characterization data.

Potassium Salt	Potassium amount (ppm)	Dispersion (%)	Surface area (BET) (m ² /g)	Pore size (nm)	Pore volume (cm ³ /g)	Reduction temperature (°C)	
						Co ₃ O ₄ →CoO	CoO→Co
None	/	7,6	133	13,1	0,45	330	403
KNO ₃	98	7,0	134	13,2	0,46	315	415
KNO ₃	267	8,1	133	13,4	0,47	320	420
KNO ₃	801	7,1	133	13,2	0,47	320	415
KNO ₃	3530	7.9	123	13.4	0.48	329	413
KCl	29	7,9	135	13,2	0,46	315	423
KCl	157	7,7	136	13,2	0,47	300	404
KCl	564	7,1	133	13,2	0,51	318	393
K ₂ CO ₃	27	7,7	127	13,3	0,46	295	404
K ₂ CO ₃	69	7,9	130	13,4	0,47	313	418
K ₂ CO ₃	464	7,5	128	13,6	0,47	303	401
K ₂ SO ₄	36	7,0	132	13,1	0,47	289	395
K ₂ SO ₄	152	7,7	131	13,2	0,47	302	403

Table 2. Estimates of the adaptive parameters contained in the deactivation expressions used for the estimation of the parameter k contained in the CO conversion model

	1	2	3
Kinetic model	$k = k_0(1 - m * K)$	$k = k_0 \exp(-m * K)$	$k = k_0 / (1 + m * K)$
m (gcat/mgκ)	-1.00E-04	-3.00E-04	6.00E-04
R ²	0.956	0.9898	0.9982
Standard error (%)	5.24	5.45	5.01

Legends for figures:

Figure 1. *Experimental setup for catalyst exposure to the aerosol particles at 300°C.*

Figure 2. *Mass size distribution of aerosol particles of potassium salts.*

Figure 3. *TPR profiles of temperature vs hydrogen consumption of standard catalyst and catalysts with different potassium loadings (KCl).*

Figure 4. *Site time yield (STY) after 24h time on stream (TOS) with different potassium salts and loadings.*

Figure 5. *C₅₊ selectivity at 50% of conversion with different potassium salts and loadings.*

Figure 6. *CH₄ selectivity at 50% of conversion with different potassium salts and loadings.*

Figure 7. *CO₂ selectivity at 50% of CO conversion with different potassium salts and loadings.*

Figure 8. *C₃ O/P selectivity at 50% of CO conversion with different potassium salts and loadings.*

Figure 9. *C₄ O/P selectivity at 50% of CO conversion with different potassium salts and loadings.*

Figure 10. *Linear regression of the deactivation rate equations.*

Figure 1. Experimental setup for catalyst exposure to the aerosol particles at 300°C

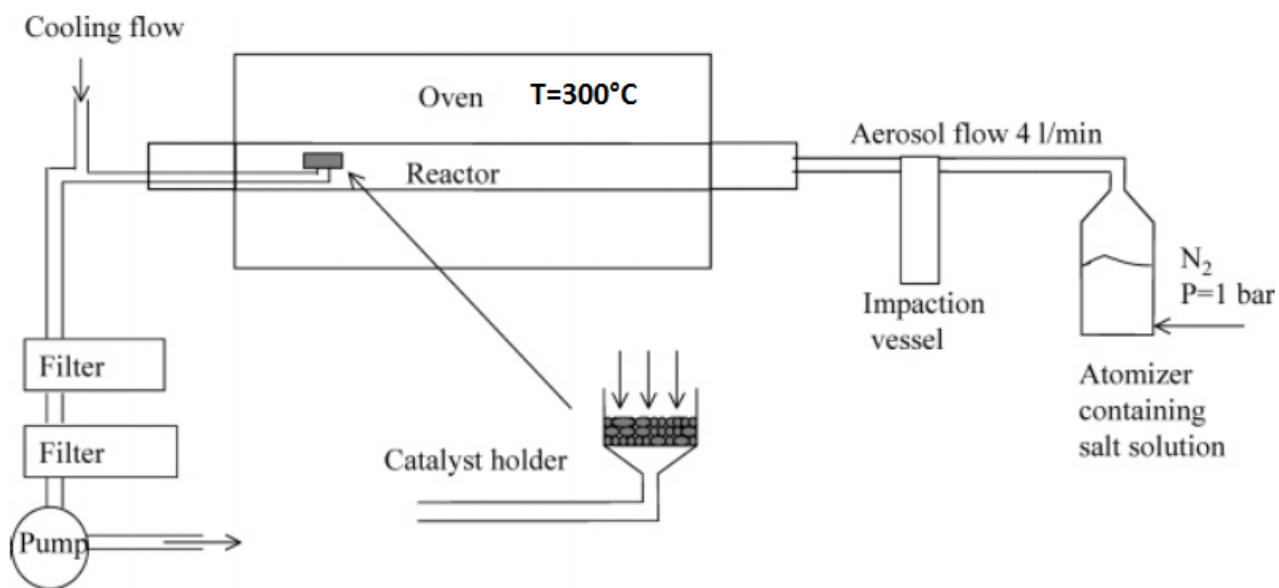


Figure 2. Mass size distribution of aerosol particles of potassium salts

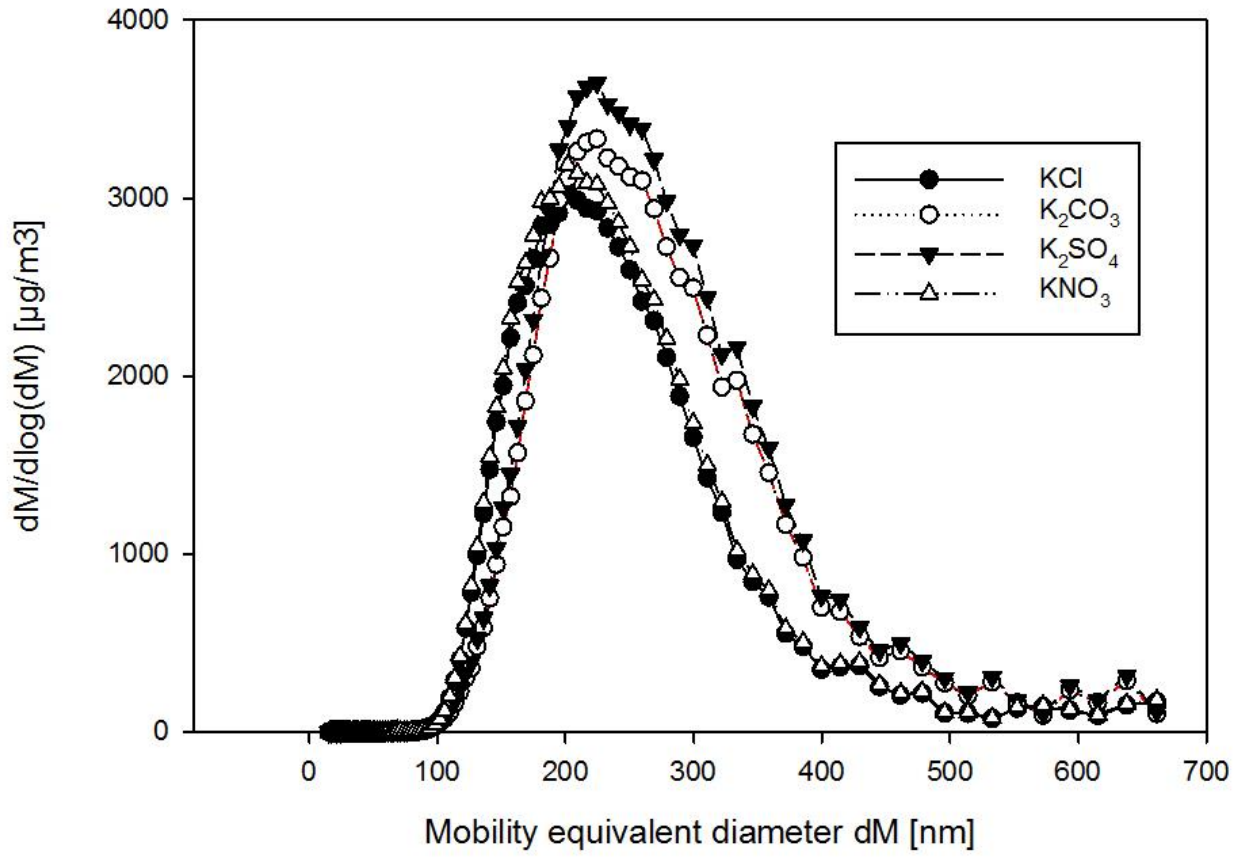


Figure 3. TPR profiles of temperature vs hydrogen consumption of standard catalyst and catalysts with different potassium loadings (KCl)

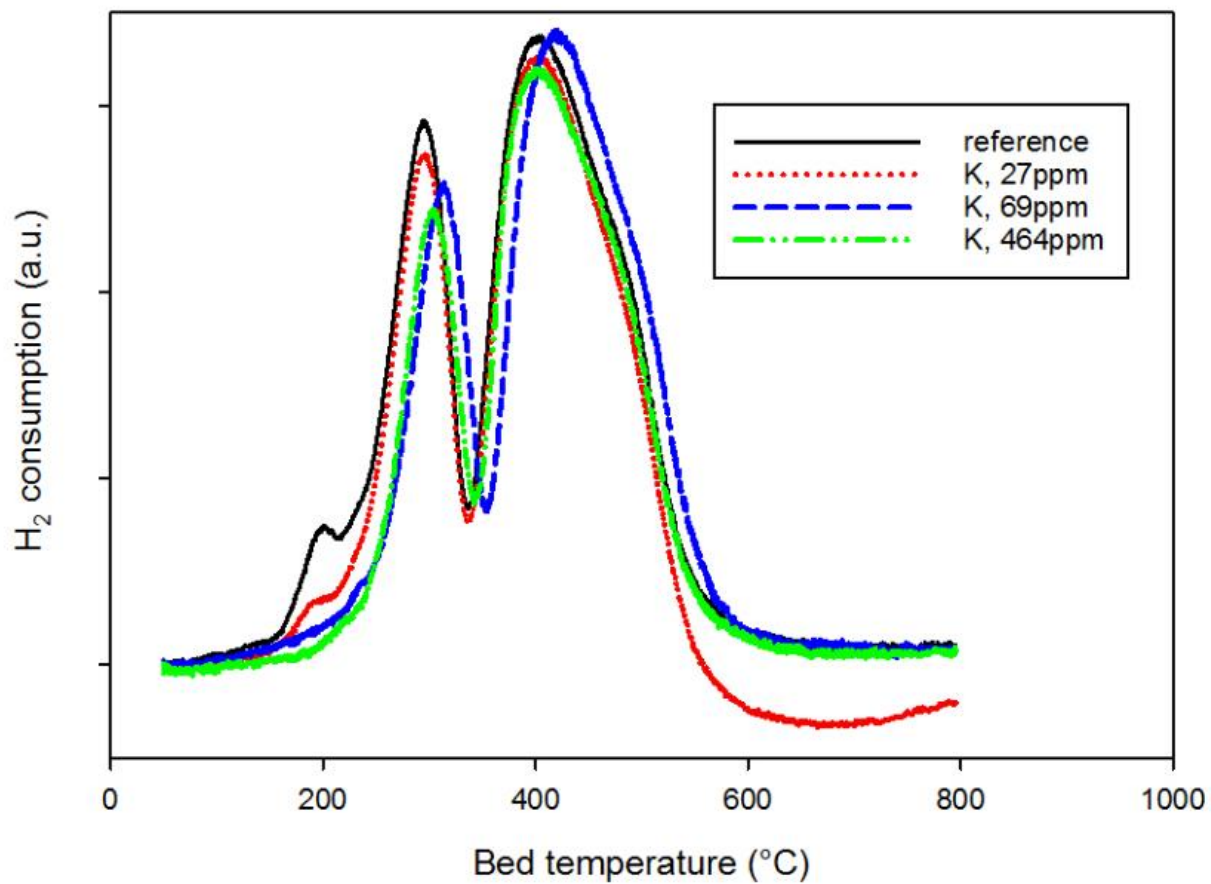


Figure 4. Site time yield (STY) after 24h time on stream (TOS) with different potassium salts and loadings

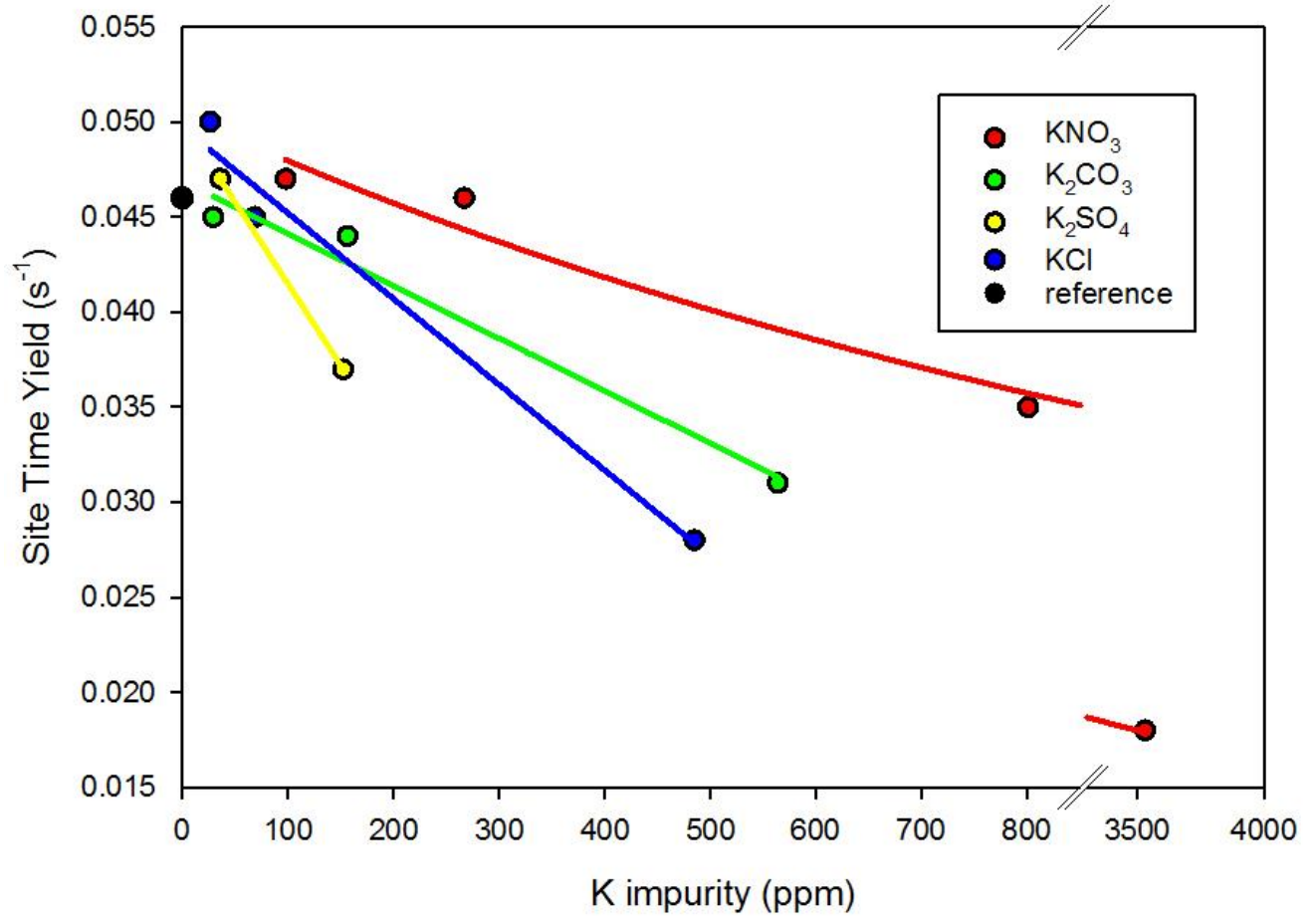


Figure 5. C_{5+} selectivity at 50% of conversion with different potassium salts and loadings

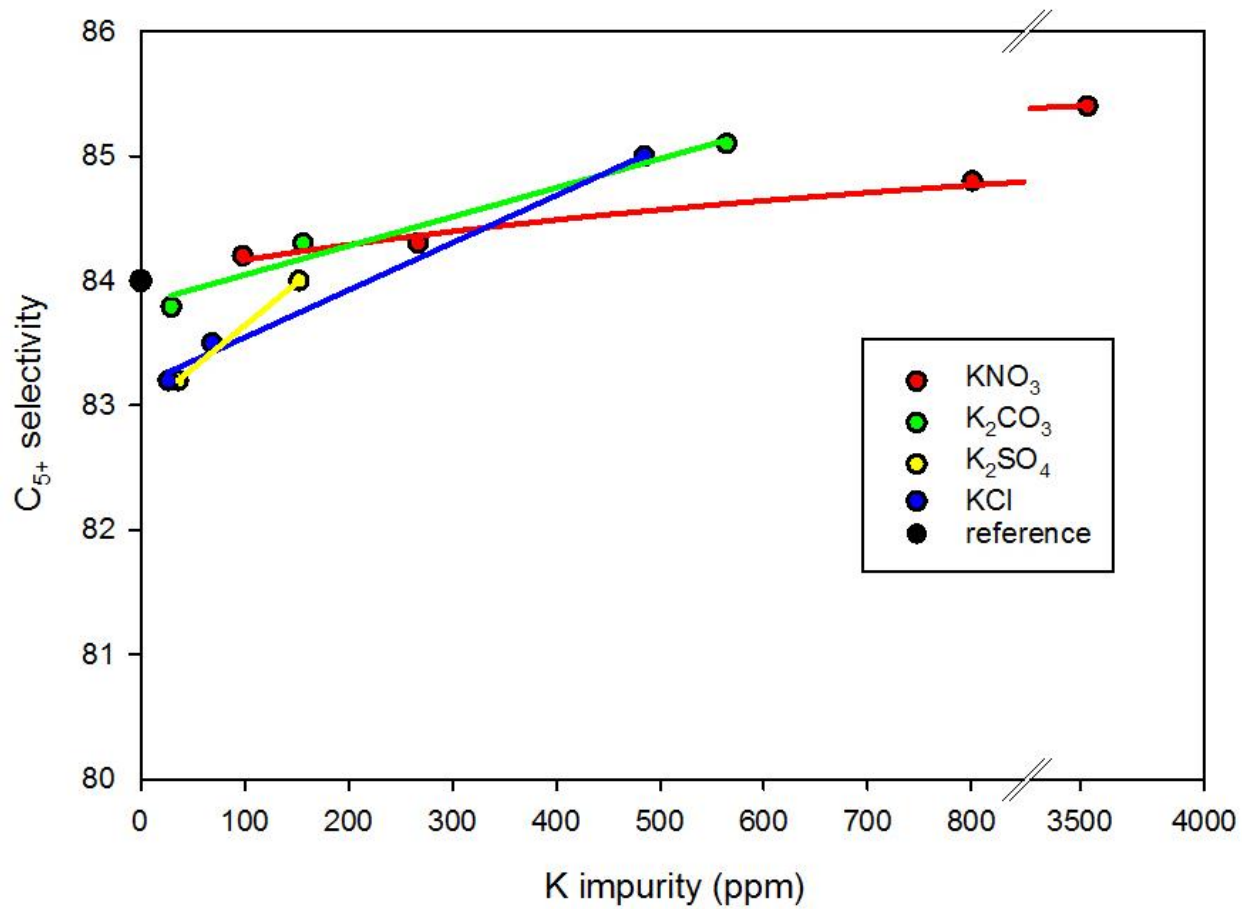


Figure 6. CH_4 selectivity at 50% of conversion with different potassium salts and loadings

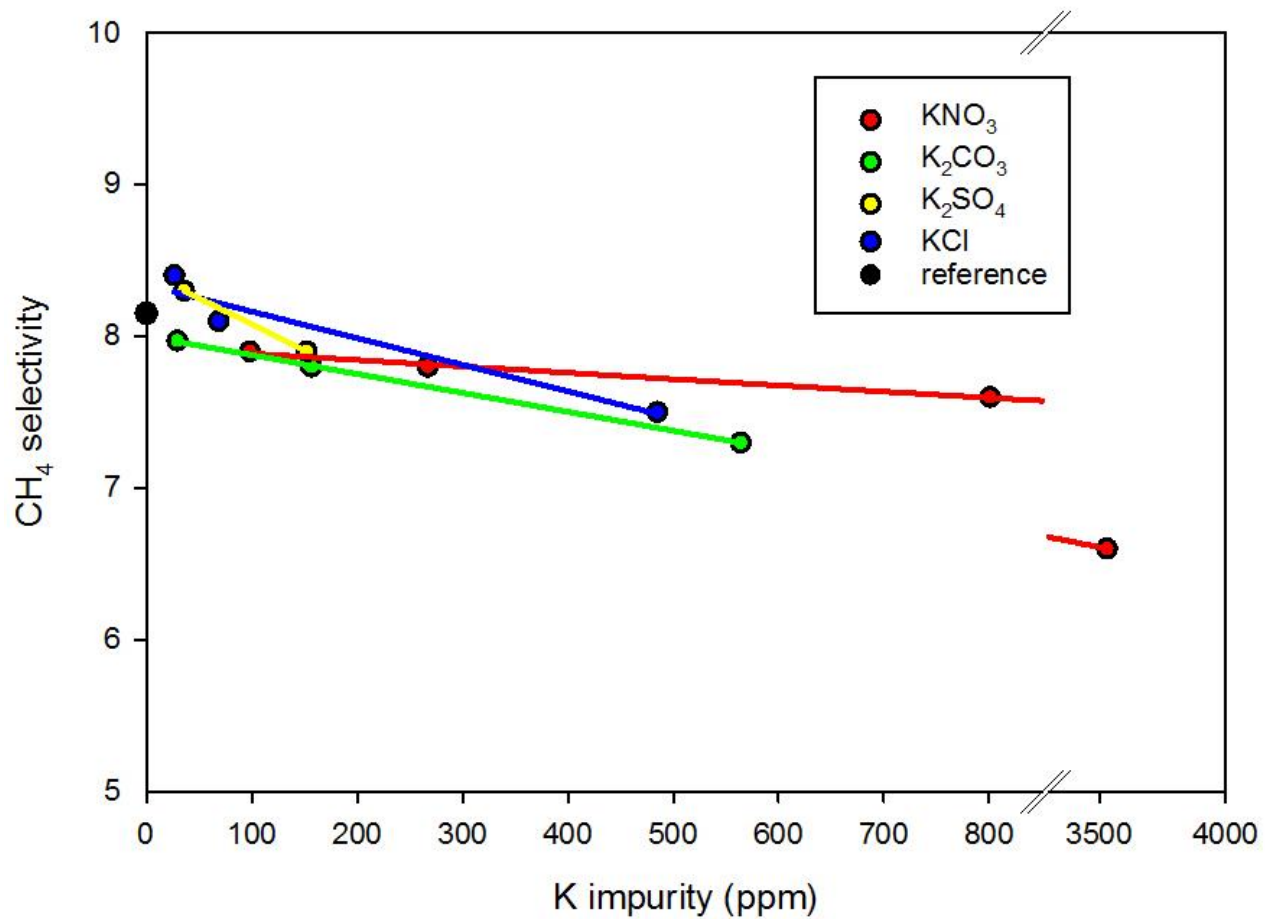


Figure 7. CO₂ selectivity at 50% of CO conversion with different potassium salts and loadings

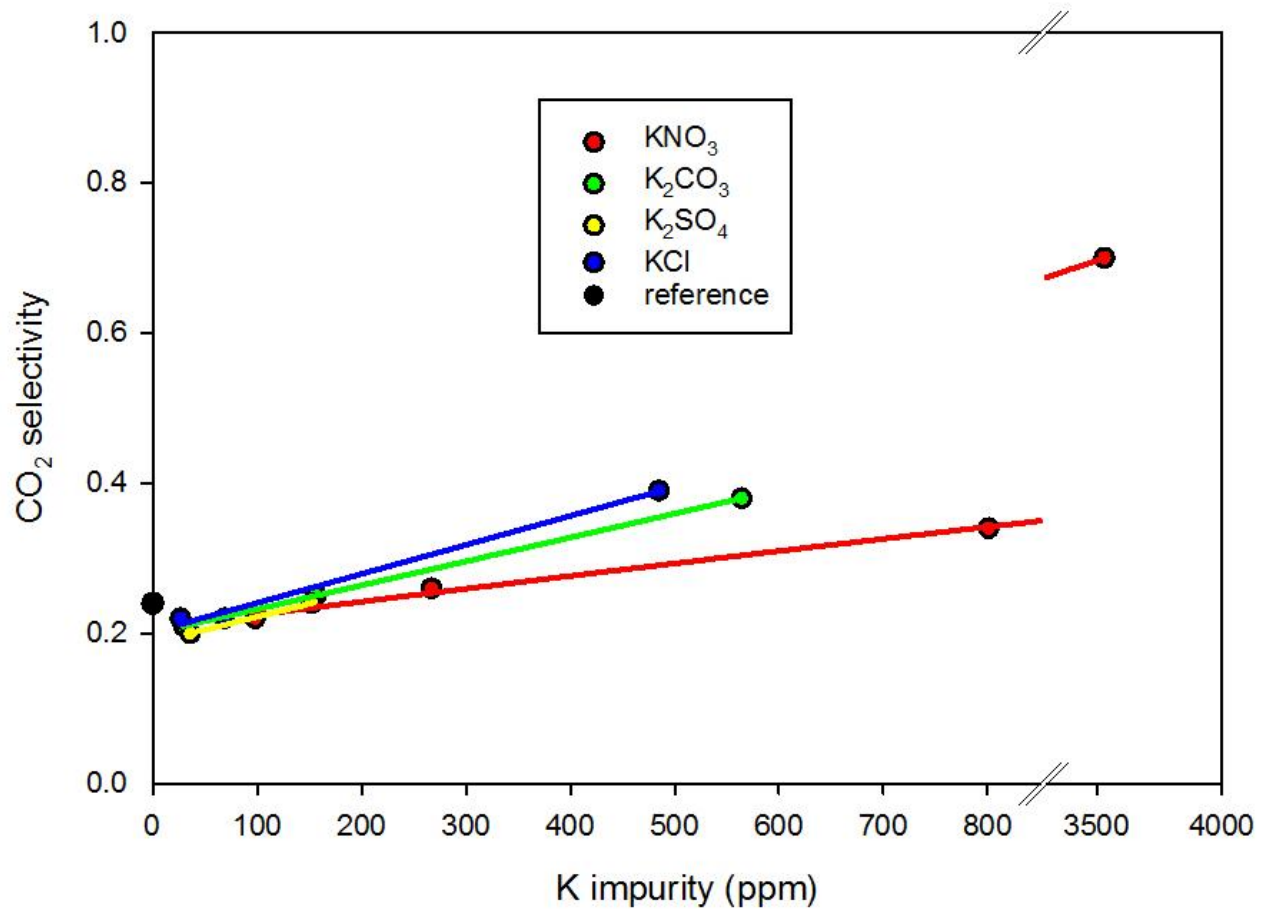


Figure 8. C₃ O/P selectivity at 50% of CO conversion with different potassium salts and loadings

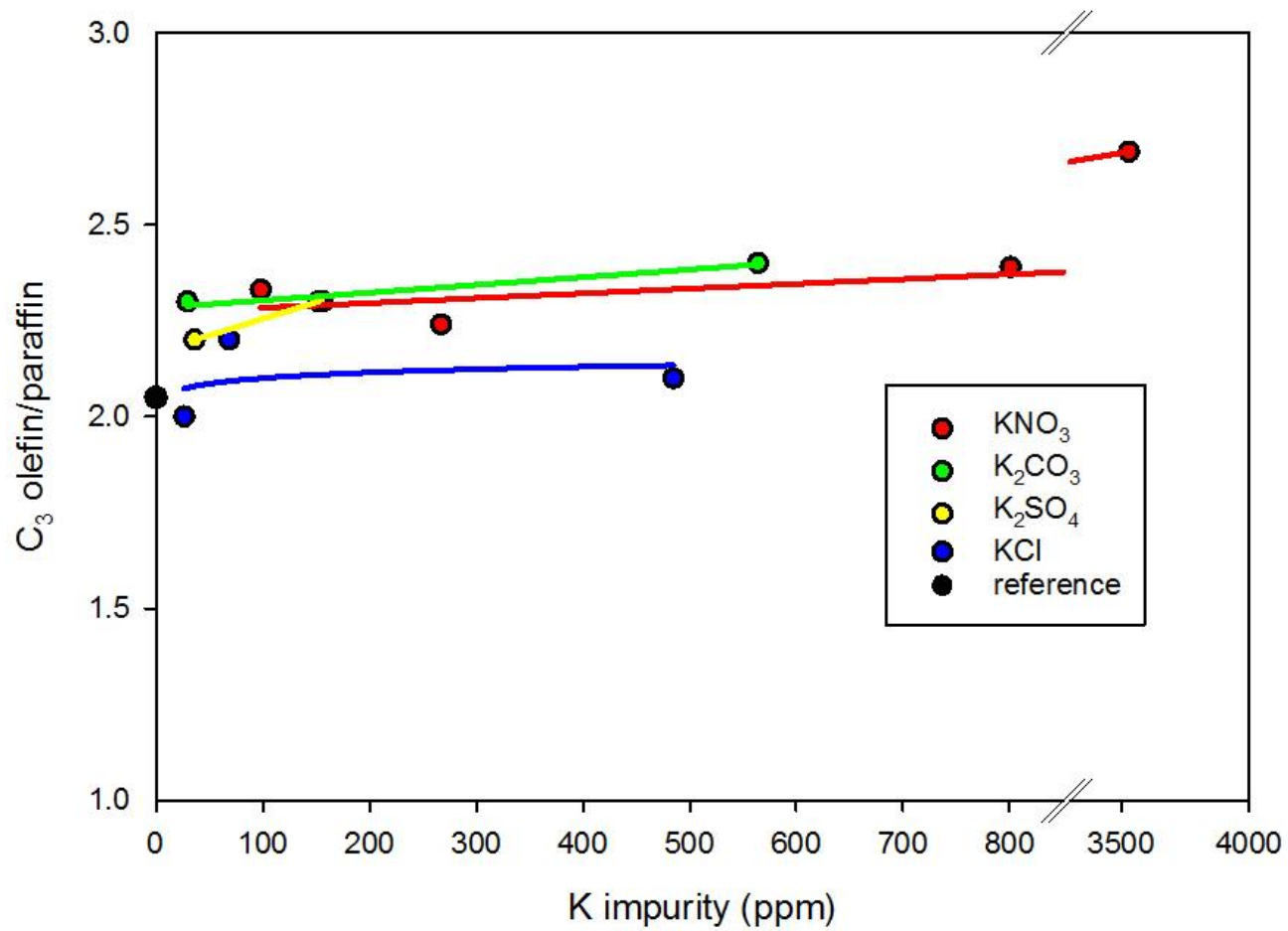


Figure 9. C₄ O/P selectivity at 50% of CO conversion with different potassium salts and loadings

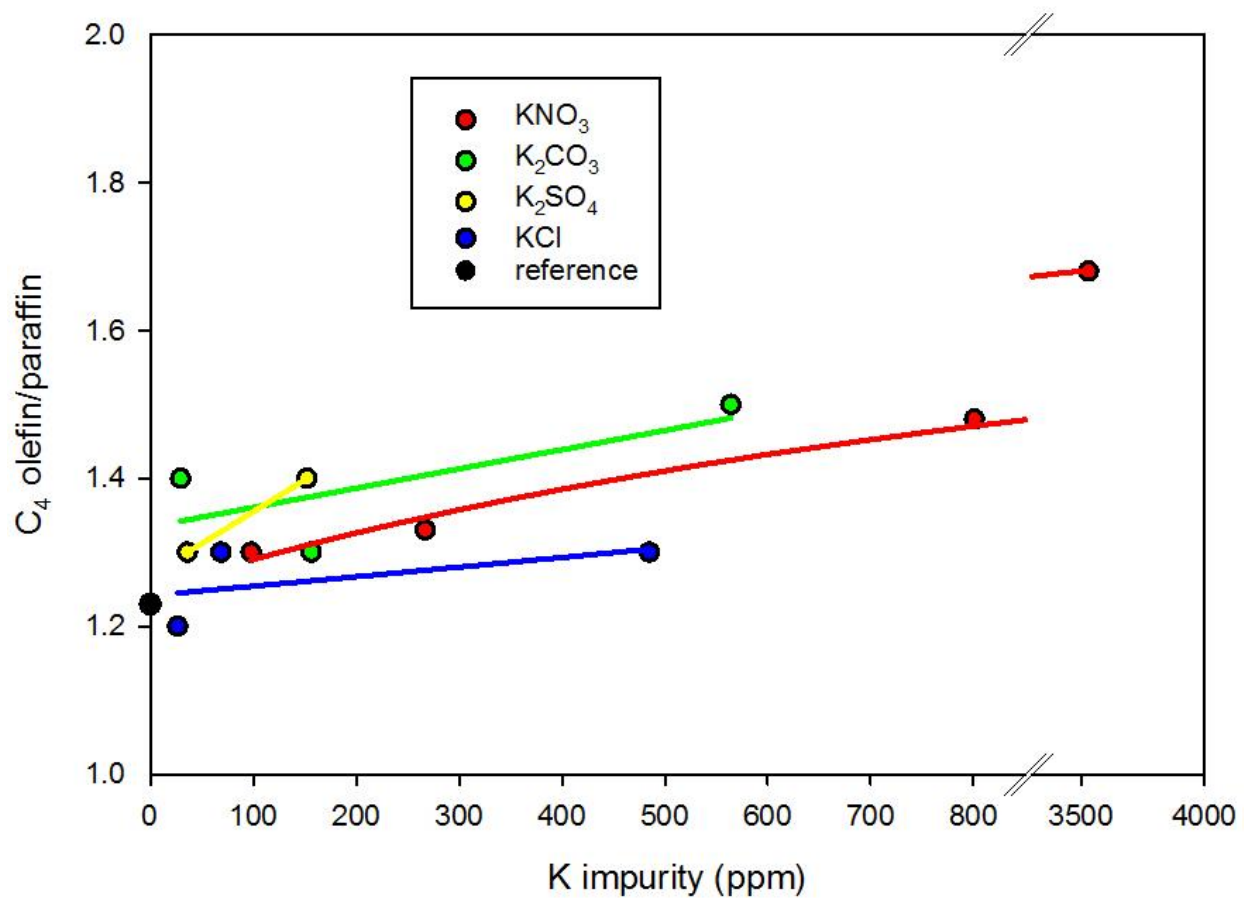
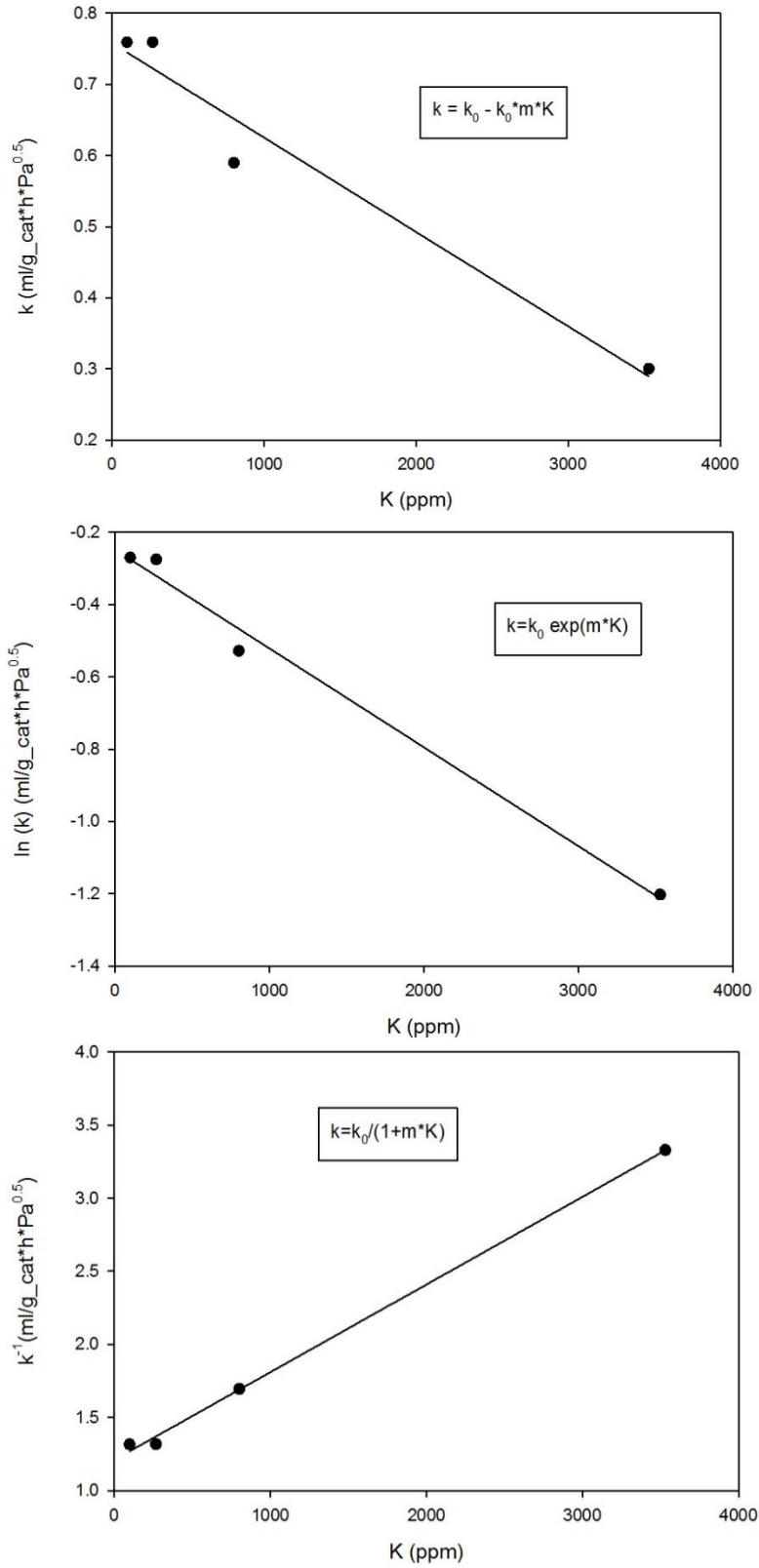


Figure 10. Linear regression of the deactivation rate equations.



Graphical abstract

